Thermoelectric power factor of ternary single-crystalline Sb_2Te_3- and Bi_2Te_3-based nanowires

2013 Nanotechnology 24 495402

(http://iopscience.iop.org/0957-4484/24/49/495402)

Nanotechnology **24** (2013) 495402 (7pp) doi:10.1088/0957-4484/24/49/495402

Thermoelectric power factor of ternary single-crystalline Sb_2Te_3- and Bi_2Te_3-based nanowires

Svenja Bäßler[1], Tim Böhnert[1], Johannes Gooth[1], Christian Schumacher[1], Eckhard Pippel[2] and Kornelius Nielsch[1]

[1] Institute of Applied Physics, University of Hamburg, Jungiusstrasse 11, D-20355 Hamburg, Germany
[2] Max Planck Institute of Microstructure Physics, Weinberg 2, D-06120 Halle, Germany

E-mail: sbaessle@physnet.uni-hamburg.de

Received 8 July 2013, in final form 27 September 2013
Published 14 November 2013
Online at stacks.iop.org/Nano/24/495402

Abstract
Nanowires of bismuth antimony telluride and bismuth telluride selenide ($Bi_{15}Sb_{29}Te_{56}$ and $Bi_{38}Te_{55}Se_7$) were grown by template-based pulsed electrodeposition. The composition and the crystallinity of the nanowires were determined by high-resolution transmission electron microscopy. The thermoelectric properties (Seebeck coefficient and electrical conductivity) of single p- and n-type nanowires, with diameter 80 nm and 200 nm, respectively, were determined as a function of temperature before and during heating in a helium atmosphere up to 300 K along the growth direction of the nanowires. After additional annealing in a tellurium atmosphere at 525 K, significantly enhanced transport properties are observed. Bulk-like power factors are achieved. In $Bi_{38}Te_{55}Se_7$ nanowires, the Seebeck coefficients increase to $-115\ \mu V\ K^{-1}$ and the thermoelectric power factors increase to $2820\ \mu W\ K^{-2}\ m^{-1}$ at room temperature. In $Bi_{15}Sb_{29}Te_{56}$ nanowires, Seebeck coefficients of up to $S = +156\ \mu V\ K^{-1}$ and power factors of up to $1750\ \mu W\ K^{-2}\ m^{-1}$ are obtained at room temperature.

S Online supplementary data available from stacks.iop.org/Nano/24/495402/mmedia

(Some figures may appear in colour only in the online journal)

1. Introduction

The efficiency of thermoelectric materials depends on the figure of merit $ZT = S^2\sigma T/\kappa$ as a function of the Seebeck coefficient S, the electrical conductivity σ, the temperature T, and the thermal conductivity κ. To date, bismuth- and tellurium-based bulk materials are still among the most promising candidates for room-temperature thermoelectric applications, due to their high figure of merit of $ZT \sim 1$ at 300 K, limiting the application of thermoelectric devices that still show a threefold lower performance than conventional energy converters [1]. It has been proposed that low-dimensional nanostructures may significantly increase the ZT. In thin nanowires, phonon surface scattering can strongly reduce the thermal conductivity, as shown by Li *et al* for Si nanowires, where a two orders of magnitude lower thermal conductivity compared to bulk material was observed [2]. This was also demonstrated by Roh *et al* for PbTe nanowires [3–5]. In addition, confinement effects have been predicted to significantly enhance the thermoelectric power factor $S^2\sigma$ beyond bulk material values [6]. Noteworthy progress has recently been made regarding the developing and characterization of binary bismuth- and tellurium-based nanowires, such as Bi_2Te_3 and Sb_2Te_3 nanowires. Although a reduction of the thermal conductivity has already been observed in these nanowires, the thermoelectric power factor is still substantially suppressed, often attributed to their low electrical conductivity due to their polycrystalline nature [7]. Successful fabrication of ternary Bi_2/Sb_2Te_3-based nanowires, such as $Bi_2(Te_xSe_{1-x})_3$ and $(Bi_{x-1}Sb_x)_2Te_3$, have been reported previously by several groups [8–10], but few publications go beyond structural characterization and focus on thermoelectric properties; see, for example, [11]. Mavrokefalos *et al* designed a platform for the measurement

of each property that is needed to calculate the complete ZT of a single nanowire [7]. In this work, we report on thermoelectric power factor measurements on individual single-crystalline $Bi_{38}Te_{55}Se_7$ and $Bi_{15}Sb_{29}Te_{56}$ nanowires grown by template-based millisecond pulsed electrochemical deposition in self-ordered Al_2O_3 membranes from an aqueous solution. The electrolyte bath and the deposition technique are related to the parameters used for the deposition of ternary thin films presented in our previous work [12]. Transmission electron microscopy shows nanowires that are single crystalline over a large range. Electrical contacts are applied to single nanowires using a lithographic method. The Seebeck coefficient and electrical conductivity are measured at temperatures between 50 and 300 K using a quasi-four-point technique. The electrical conductivity of the nanowires is measured in the growth direction, since this was not possible for the thin films presented in our previous work, where the electrical conductivity was measured perpendicular to the growth direction [12]. The nanowires were annealed in a helium atmosphere, and a reduction of the number of crystal defects, leading to a higher thermoelectric performance, was expected. In order to further improve the nanowires' compositions and their thermoelectric performance, they were annealed in a tellurium atmosphere, since this led to a better thermoelectric performance of the thin films [12].

2. Synthesis and characterization methods

2.1. Nanowire synthesis

The nanowires were electrodeposited into porous alumina templates using a millisecond pulsed voltage. To achieve highly ordered pores, a two-step anodization process was used to prepare the templates for the electrodeposition [13, 14]. Aluminum with a purity of 99.999% was anodized in phosphoric acid, forming membranes with an average pore diameter of 200 nm, interpore distances of about 420 nm, and a pore length of at least 50 μm. A gold film was sputtered on the backside of the membrane, followed by a gold deposition, acting as cathode for the electrodeposition of the nanowires using a three-electrode setup. A platinum mesh builds the anode, and a Ag/AgCl reference was used. $Bi_{38}Te_{55}Se_7$ and $Bi_{15}Sb_{29}Te_{56}$ nanowires were deposited into the pores of the alumina membrane from aqueous solutions ($Bi_{38}Te_{55}Se_7$: 1 mol l^{-1} nitric acid with 0.01 mol l^{-1} TeO_2, 0.01 mol l^{-1} $Bi(NO_3)_3$ + 5 H_2O and 0.0011 mol l^{-1} SeO_2/$Bi_{15}Sb_{29}Te_{56}$: 1 mol l^{-1} nitric acid with 0.007 mol l^{-1} TeO_2, 0.002 mol l^{-1} $Bi(NO_3)_3$ + 5 H_2O, and 0.006 mol l^{-1} Sb_2O_3, with 0.9 mol l^{-1} tartaric acid) using a *Bio-Logic VSP potentiostat* with millisecond voltage pulses. The on-/off-time was 10 ms/50 ms; during the on-time, a potential of −0.18 V for $Bi_{38}Te_{55}Se_7$ and −0.34 V for $Bi_{15}Sb_{29}Te_{56}$ and during the off-time the open circuit potential was applied. All process parameters except the deposition potential were optimized for the thermoelectric performance of electrodeposited thin films, leading to film compositions of about 40% Bi, 50% Te, 10% Se and 30% Sb, 10% Bi, and 60% Te, respectively, within an error of about 5% determined by ICP-OES [15]. Compared to the thin film synthesis, the diffusion path is longer and is one dimensional in alumina membranes, due to the given pore structure, causing a shift in the deposition potentials. Further details of the deposition have been reported in our previous work regarding $Bi_2(Te_xSe_{1-x})_3$ and $(Bi_{x-1}Sb_x)_2Te_3$ thin films [12]. To release the nanowires from the template, the alumina membranes were selectively dissolved by a solution of chromic and phosphoric acid. After rinsing in deionized water, the nanowires were suspended in ethanol.

2.2. Measurements

The nanowire dispersion was placed drop-wise onto a glass substrate for Seebeck coefficient and electrical conductivity measurements. A photoresist mask for applying electrical contacts to the nanowires was defined via standard laser beam lithography (laserwriter model *μPG* 101 by *Heidelberg Instruments*) and by subsequent development of the exposed photoresist. In order to remove residues and the barrier-oxide layer on the nanowire surface, Ar plasma etching was performed prior to sputtering of Ti/Pt contacts and the lift-off process. The contact material was platinum. The Seebeck coefficients and the electrical conductivities of the as-deposited nanowires were measured in steps of 25 K in the range 50–300 K at constant temperatures in a *VERSALAB Physical Property Measurement System (Quantum Design)* equipped with an *electrical-transport measurement option* in a helium atmosphere. Subsequently, the cryostat was heated to 400 K and a few milliwatts were applied to the microheater for about 15 min in order to avoid irreversible changes during the Seebeck coefficient measurement. The average temperature of the nanowire during this heat treatment was determined by calibrated thermometers to be about 425 K. Afterwards, the Seebeck coefficient and electrical conductivity of the nanowire were measured again from 50 to 300 K. In order to understand the changes in the thermoelectric properties observed during heating from the as-prepared state to approximately 425 K, the change of the electrical conductivity was monitored at different temperature steps. To obtain the Seebeck coefficient $S = -U_{\mathrm{th}}/\Delta T$, an on-chip microheater near the nanowire was used to generate a small temperature gradient ΔT across its length. ΔT was determined by the resistive change $\mathrm{d}R/\mathrm{d}T$ of two metallic thermometer lines located at the nanowire margins. For each thermometer, a four-terminal lock-in technique was used, in which a sinusoidal excitation current of 10 μA was applied. The two thermometers were driven at distinct frequencies of 128 and 186 Hz to avoid cross-talk. The thermometers were calibrated during the measurement against the base temperature of the cryostat. The thermovoltage U_{th} was measured between the nanowire's ends using the two thermometers as probes. The conductance of the nanowire was determined in a quasi-four-point configuration with a conventional lock-in technique. An active feedback driven AC current $I_{\mathrm{ap}} = 1$ μA was applied through the nanowire and the voltage drop U_{meas} along the nanowire was measured. The electrical conductivity was calculated using $\sigma = (4I_{\mathrm{ap}}l)/(U_{\mathrm{meas}}\pi d^2)$; the measured length of the nanowire $l \sim (8 \pm 0.1)$ μm

and the nanowire diameter $d = (200 \pm 20)$ nm. To account for the roughness of the $Bi_{15}Sb_{29}Te_{56}$ nanowires, we assumed an effective diameter $d = (80 \pm 40)$ nm for the conductivity calculations, which was a rough estimation based on transmission electron microscopy and scanning electron microscopy images/measurements, leading to high errors in the determination of the electrical conductivity. In order to calculate the mobility of the nanowires, two-point resistance measurements on the nanowires were performed, with a constant voltage source in the back-gate device geometry. For these measurements, the nanowires were placed on a highly doped silicon substrate with a 200 nm silicon oxide layer and the electrical contacts were defined using laser beam lithography, as described above. The measurement procedure has been described elsewhere [16].

2.3. Annealing in a tellurium atmosphere

The nanowires were annealed in a tellurium atmosphere as described by Rostek *et al* to improve their composition [17]. For the annealing process, nanowires were placed drop-wise on a glass substrate. This substrate and pure tellurium powder were heated up to the annealing temperature of 525 K for 60 h in an evacuated glass tube. With these parameters, equilibrium conditions can be achieved. If the material is Bi rich, it reacts with the Te of the gas phase; if it is Te rich, the Te excess evaporates, and the composition of the material can be improved [17].

3. Results and discussion

The crystallinity and the composition of the nanowires were determined by transmission electron microscopy (TEM) including energy dispersive x-ray analysis (EDX). The nanowires were shown to be $Bi_{38}Te_{55}Se_7$ and $Bi_{15}Sb_{29}Te_{56}$ by TEM-EDX with an error of approximately 5%. Both types of nanowire were single crystalline over a large range, as exemplarily shown in high-resolution TEM images (figures 1(a) and (b); see also figures 4 and 5 in the supporting information available at stacks.iop.org/Nano/24/495402/mmedia).

While the geometry of the $Bi_{38}Te_{55}Se_7$ nanowires is a well-defined homogeneous cylinder with a diameter of approximately 200 nm, the $Bi_{15}Sb_{29}Te_{56}$ nanowires exhibit vacancies in the nanowires (figure 1(c)) due to a dendrite crystal growth. These vacancies reduce the surface of the cross section and therefore the nanowire conductance. A scanning electron microscope micrograph of a typical device for thermoelectric characterization of single nanowires is presented in figure 1(d). It consists of a microheater (top) and two quasi-four-point thermometers at the nanowire. With this structure, the temperature-dependent Seebeck coefficient and electrical conductivity of the nanowires can be measured. In addition, the charge carrier mobility and concentration of the nanowires are calculated using a nanowire transistor configuration.

Figures 2(a)–(c) show the Seebeck coefficient (a), the electrical conductivity (b), and the thermoelectric power factor (c) of an individual single-crystalline $Bi_{15}Sb_{29}Te_{56}$ nanowire as a function of temperature between 50 and 300 K.

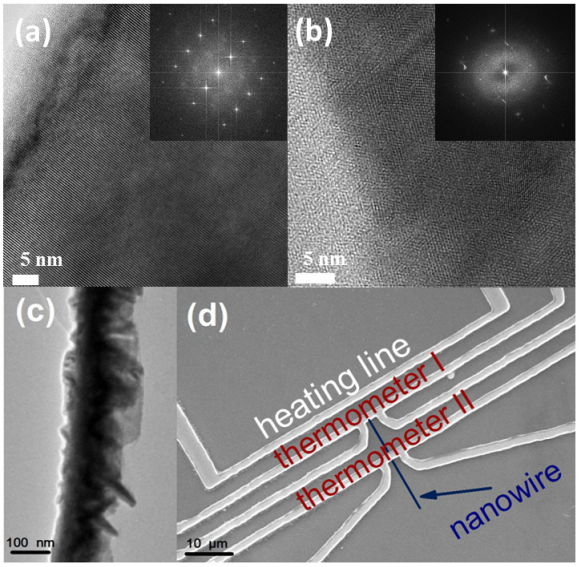

Figure 1. High-resolution TEM (HRTEM) images of single (a) $Bi_{38}Te_{55}Se_7$ and (b) $Bi_{15}Sb_{29}Te_{56}$ nanowires with the corresponding diffraction images as the inset. (c) shows an overview of the typical morphology of the $Bi_{15}Sb_{29}Te_{56}$ nanowires, which shows the vacancies in the nanowire. The contact pattern of the Seebeck measurement contacts is shown in (d).

The light grey squares display the as-prepared data and an irreversible conductance change during heating above room temperature (RT), while the dark grey squares show the reversible thermoelectric properties after heating. The nanowire shows p-type transport over the whole temperature range, indicated by a positive Seebeck coefficient and confirmed by the slope of the resistance versus gate voltage curve of the gate measurements (see supporting information available at stacks.iop.org/Nano/24/495402/mmedia). The Seebeck coefficient decreases linearly with decreasing temperature and extrapolates to zero at $T = 0$ K. For temperatures approaching RT, the slope decreases and gets saturated above RT. This behaviour may be explained due to approach of the intrinsic region and mixing of electron and hole conduction [18]. This results in a maximum Seebeck coefficient of $+127$ μV K^{-1} for the as-deposited nanowire at 300 K. After heating in a helium environment, this value is slightly enhanced to $+135$ μV K^{-1}, which is still low compared to the nanograined bulk ($S_{\mathrm{bulk}} = +210$ μV K^{-1}) and in the region of that for as-prepared electrodeposited $(Bi_{x-1}Sb_x)_2Te_3$ thin films ($S_{\mathrm{film}} = +135$ μV K^{-1}) [12, 19, 20]. The heating process causes a drop of the electrical conductivity from 960 to 640 S cm^{-1} at 300 K, most likely due to the healing of defects, leading to a lower carrier concentration and therefore a lower electrical conductivity. A similar trend was observed in previous measurements on electrodeposited films, with the same deposition parameters, where the electrical conductivity at room temperature decreased from 560 to 400 S cm^{-1} [12]. Significantly higher electrical conductivities of 1250 S cm^{-1} at 300 K have been reported for nanograined bulk $(Bi_{x-1}Sb_x)_2Te_3$ [19]. The large

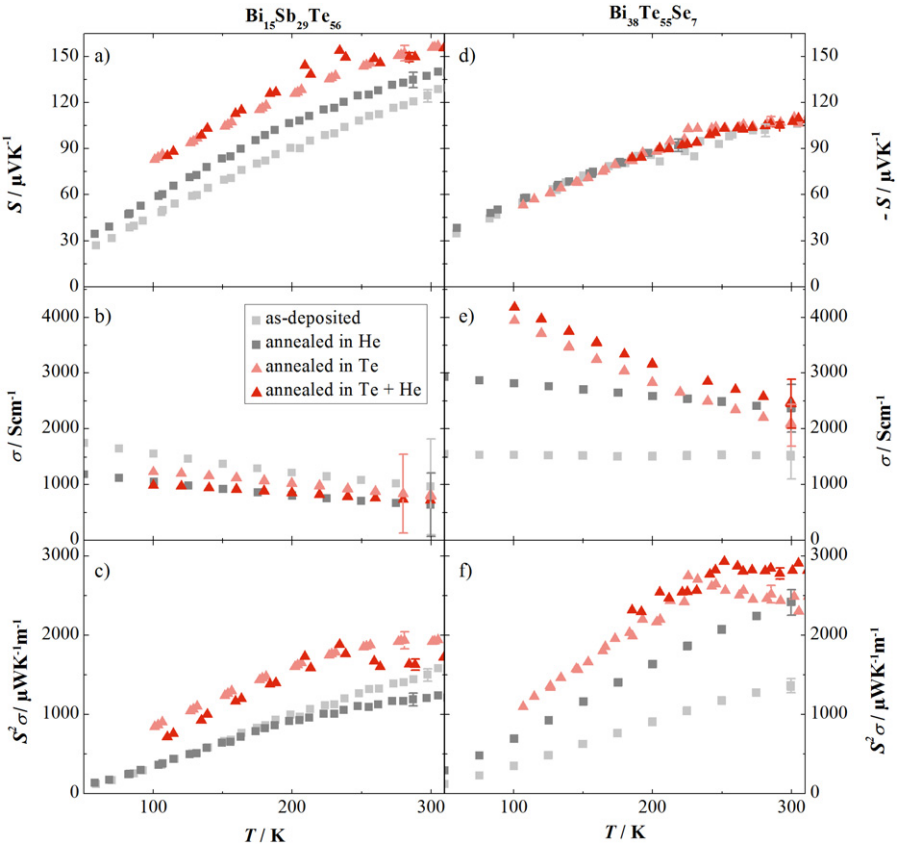

Figure 2. (a) Seebeck coefficient, (b) electrical conductivity, and (c) thermoelectric power factor of a single 200 nm thick $Bi_{38}Te_{55}Se_7$ nanowire as a function of temperature. The corresponding values for the $Bi_{15}Sb_{29}Te_{56}$ nanowires are shown in (d)–(f). The nanowires were measured from 50 to 300 K, then heated in the cryostat to 425 K, and the measurement was repeated. Results for as-deposited (light grey), helium-annealed (dark grey), tellurium-annealed (light red), and tellurium-annealed and subsequently helium-annealed (red) nanowires are shown. Due to the modulated surface based on the plate-like growth, the conductive values are approximated for an effective diameter of 80 nm. Error bars are exemplarily shown for selected data points.

Table 1. Thermoelectric properties of bulk, thin film, and nanowire $(Bi_{1-x}Sb_x)_2Te_3$ as well as $Bi_2(Te_xSe_{1-x})_3$ materials.

	p-type $(Bi_{1-x}Sb_x)_2Te_3$			n-type $Bi_2(Te_xSe_{1-x})_3$		
	S (μV K^{-1})	σ (S cm^{-1})	$S^2\sigma$ (mW K^{-2} m^{-1})	S (μV K^{-1})	σ (S cm^{-1})	$S^2\sigma$ (mW K^{-2} m^{-1})
Nanograined bulk [18, 22]	+210	1250	4700	−220	770	2600
Thin films [12]						
As deposited	+135	560	1021	−82	702	472
Te annealed	+182	400	1325	−130	488	825
Nanowires						
As deposited	+127 ± 4	960 ± 860[a]	1550 ± 80	−105 ± 4	1300 ± 420	1500 ± 90
After heating	+135 ± 5	640 ± 570[a]	1170 ± 80	−105 ± 4	2300 ± 430	2500 ± 160
Te-annealed nanowires						
As prepared	+156 ± 5	790 ± 710[a]	1920 ± 110	−115 ± 3	1990 ± 370	2660 ± 110
After heating	+156 ± 3	720 ± 640[a]	1750 ± 70	−115 ± 2	2200 ± 440	2820 ± 70

[a] Large errors are caused by the errors in the determination of the nanowires' diameter due to their irregular shape.

error bars for the electrical conductivity are caused by the high errors in the nanowires' diameter due to the irregular shape of the p-type nanowires. The room-temperature power factor ($S^2\sigma$ = 1170 μW K^{-2} m^{-1}) of the $Bi_{15}Sb_{29}Te_{56}$ nanowire is still far away from nanograined bulk values ($S^2\sigma_{bulk}$ = 4700 μW K^{-2} m^{-1}) [19], but reaches the region of values for as-prepared electrodeposited films ($S^2\sigma_{film}$ = 1021 μW K^{-2} m^{-1}) [12]. This nanowire shows a decreasing power factor after heat treatment due to the strong reduction of the electrical conductivity. A summary of these results can be found in table 1.

Figures 2(a)–(c) also show the Seebeck coefficient (a), the electrical conductivity (b), and the thermoelectric power factor (c) of an individual single-crystalline $Bi_{15}Sb_{29}Te_{56}$

nanowire after annealing in a tellurium atmosphere before (light red triangles) and after (red triangles) heating in a helium atmosphere. The Seebeck coefficient and the electrical conductivity show the same behaviour as for the as-deposited nanowires but the Seebeck coefficient reaches higher values of about $+156\ \mu V\ K^{-1}$ at RT. After heating, there is no change in the behaviour of the Seebeck coefficient. The electrical conductivity shows slightly lower values compared to the as-deposited nanowire (790 S cm^{-1} and 720 S cm^{-1} at RT before and after heating up, respectively). These values result in a power factor of about 1920 $\mu W\ K^{-2}\ m^{-1}$ at RT before (and 1750 $\mu W\ K^{-2}\ m^{-1}$ after) heating up in a helium atmosphere. This is an improvement of about 40% compared to nanowires not annealed in tellurium, and can be explained by changes in the composition due to the tellurium annealing process (see table 1). In earlier works, it was shown that the thermoelectric performance strongly depends on the composition of the materials [21]. The annealing of ternary Bi_2Te_3-based thin films has already been investigated; it was reported that annealing for 60 h at 525 K in a tellurium atmosphere can improve the composition of the thin films significantly, leading to a 30% higher thermoelectric performance [12, 16]. The composition of the nanowires presented here changes during annealing. Since the material shows a lack of tellurium, an increase of the tellurium amount can be expected after annealing in tellurium, leading to an optimized material. Compared to that of annealed thin films, the power factor of the annealed nanowires presented here is 30% higher. A significant change in the morphology of the nanowires (especially the p-type wires with the irregular shape) due to the annealing process was not observed (see also supporting information available at stacks.iop.org/Nano/24/495402/mmedia).

Figures 2(d)–(f) show the Seebeck coefficient (d), the electrical conductivity (e), and the thermoelectric power factor (f) in the same temperature range for an individual single-crystalline $Bi_{38}Te_{55}Se_7$ nanowire before (light grey squares) and after (dark grey squares) heating in a helium atmosphere. The Seebeck coefficient is negative over the whole temperature range, indicating n-type transport, which is confirmed by gate measurements due to the slope of the resistance versus gate voltage curve (see supporting information available at stacks.iop.org/Nano/24/495402/mmedia). Its value behaves similarly with respect to the temperature as observed for the $Bi_{15}Sb_{29}Te_{56}$ nanowire, resulting in a maximum Seebeck coefficient of $-105\ \mu V\ K^{-1}$ nanowire at 300 K with negligible change after heating to 425 K. The Seebeck coefficient reported here is still suppressed compared to nanograined bulk values (S_{bulk} (300 K) $= -220\ \mu V\ K^{-1}$) [22] and enhanced compared to the thermopower of as-prepared electrodeposited films (S_{film} (300 K) $= -82\ \mu V\ K^{-1}$) and single-crystalline Bi_2Te_3 nanowires ($S_{Bi_2Te_3NW}$ (300 K) $= -53\ \mu V\ K^{-1}$) [12, 7]. The as-prepared sample's electrical conductivity shows almost no temperature dependence up to RT, with an average value of 1300 S cm^{-1}. After heating to higher temperatures the electrical conductivity irreversibly increases to 2300 S cm^{-1} at 300 K, contrary to the observation for $Bi_{15}Sb_{29}Te_{56}$. This enhancement may be attributed to the reduction of the number of defects during the annealing process and therefore to a higher mobility, as discussed later. The room-temperature electrical conductivity of the $Bi_{38}Te_{55}Se_7$ nanowire is significantly higher than the values reported for nanograined bulk material at 300 K ($\sigma_{bulk} = 770$ S cm^{-1}) [22] and values for electrodeposited $Bi_2(Te_xSe_{1-x})_3$ films of 700 S cm^{-1} [12], but comparable to that of single-crystalline Bi_2Te_3 nanowires ($\sigma_{Bi_2Te_3NW} =$ 2150 S cm^{-1}) [12]. Bismuth telluride is known to have an anisotropic electrical conductivity which depends on the alloy. The electrical conductivity is three to six times lower along the *c*-axis compared to the perpendicular axis [23]. Compared to polycrystalline isotropic bulk a two to four times higher electrical conductivity along the growth direction and perpendicular to the *c*-axis can be expected, due to the random orientated crystallites in the polycrystalline bulk, leading to a higher average electrical resistance. The deviation of our single-crystalline $Bi_{38}Te_{55}Se_7$ nanowires from the bulk value can be explained by the differences in their crystallinity and no additional doping. It was already shown that millisecond pulsed electrodeposited single-crystalline Bi_2Te_3 nanowires grow perpendicular to the direction of the *c*-axes (111) in the (110) direction [24–26] and that for $Bi_{38}Te_{55}Se_7$ thin films (110) is the preferred growth direction [12] as well as for $Bi_2(Te_xSe_{1-x})$ nanowires [27]. Therefore it can be assumed that the transport properties of the nanowires presented here are measured in the growth direction, meaning perpendicular to the *c*-axis, leading to the high electrical conductivity. For Sb_2Te_3-based materials, the (015) direction is the preferred growth direction, but x-ray diffraction measurements show also a ratio perpendicular to the *c*-axis in the (110) direction [12, 28]. As a result, the electrical conductivity in $Bi_{15}Sb_{29}Te_{56}$ nanowires is lower compared to that in n-type nanowires. In general, one would expect that the electrical conductivity in nanowires is suppressed compared to the bulk, due to enhanced boundary scattering in nanostructures in the diffusive transport regime. Therefore, it seems that the electrical conductivity is dominated by the influence of the anisotropic effects. The thermoelectric power factor $S^2\sigma$ of the $Bi_{38}Te_{55}Se_7$ nanowire was calculated, and after heating up, the power factor was two times larger, resulting in a maximum value of 2500 $\mu W\ K^{-2}\ m^{-1}$ at 300 K. This value is comparable to that of nanograined bulk ($S^2\sigma_{bulk}$ (300 K) $= 2600\ \mu W\ K^{-2}\ m^{-1}$) [22], and is approximately 400% improved compared to values for as-prepared electrodeposited films ($S^2\sigma_{film}$ (300 K) $=$ 472 $\mu W\ K^{-2}\ m^{-1}$) and single-crystalline Bi_2Te_3 nanowires ($S^2\sigma_{Bi_2Te_3NW}$ (300 K) $= 600\ \mu W\ K^{-2}\ m^{-1}$) [12, 7]. A summary of the results for $Bi_{38}Te_{55}Se_7$ is presented in table 1.

From two-point measurement data, charge carrier mobilities μ in the region of 24 $cm^2\ V^{-1}\ s^{-1}$ and 34 $cm^2\ V^{-1}\ s^{-1}$ and carrier concentrations n/p of 2.7×10^{20} cm^{-3} and 2.1×10^{20} cm^{-3} were achieved at room temperature for $Bi_{38}Te_{55}Se_7$ and $Bi_{15}Sb_{29}Te_{56}$ nanowires, respectively. Measurements were performed using the conventional back-gate nanowire field effect transistor model [16]. At almost similar conditions, electrochemically deposited thin films

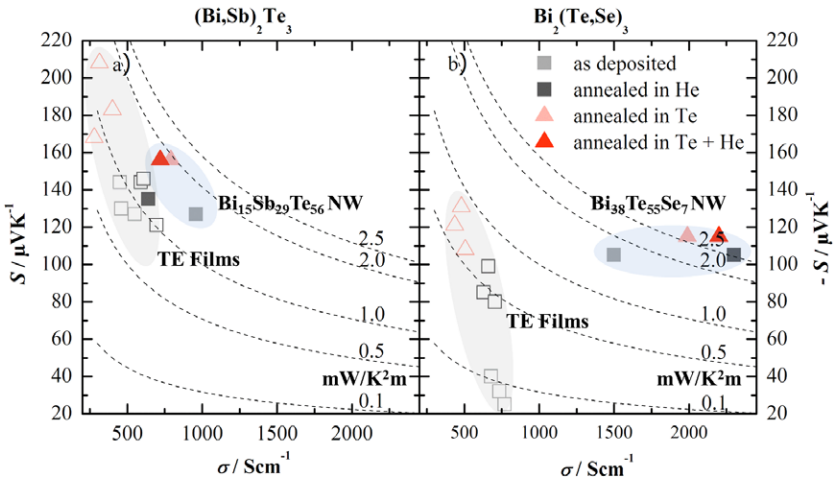

Figure 3. The dependence of the Seebeck coefficient of thin films (open symbols) and nanowires (filled symbols) for (a) $Bi_{15}Sb_{29}Te_{56}$ and (b) $Bi_{38}Te_{55}Se_7$ on the electrical conductivity. The dashed lines mark equal power factors. The thin film data were published by Schumacher *et al* [12].

had comparable carrier concentrations, but showed a slightly lower mobility ($\mu_{\text{film}} \sim 11$ cm^2 V^{-1} s^{-1}), most likely because of enhanced scattering at the grain interfaces in the polycrystalline films [12].

Figures 2(d)–(f) additionally show the Seebeck coefficient (d), the electrical conductivity (e), and the thermoelectric power factor (f) of an individual single-crystalline $Bi_{38}Te_{55}Se_7$ nanowire after annealing in a tellurium atmosphere (light red triangles; the red triangles show measurements after additional heating in helium). The Seebeck coefficient exhibits the same n-type behaviour as the as-grown nanowire, but reaches slightly higher values of about -115 μV K^{-1} at RT; the electrical conductivity before additional heating in helium is improved compared to the value for nanowires not annealed in tellurium (1990 S cm^{-1}), and is comparable after heating up (2200 S cm^{-1}). This leads to power factors of about 2820 μW K^{-2} m^{-1} after heating, which is an improvement of about 13% of the value of the nanowire not annealed in tellurium after heating (see also table 1). Here, two effects may occur during annealing. The selenium evaporates during the process due to its low vapour pressure, and the Bi–Te-ratio is adjusted to 2:3 [12]. Regarding thin films, a significant improvement may be achieved due to annealing in a tellurium atmosphere: the power factor reaches a value of 825 μW K^{-2} m^{-1} [12]. This value is a factor of 2.4 lower than the value presented here for nanowires, most likely due to their high electrical conductivity.

Figure 3 displays the dependence of the Seebeck coefficient on the electrical conductivity at room temperature, to compare the results for nanowires (filled symbols) to the results of thin films (open symbols). Values for the as-deposited and the (in tellurium and helium atmosphere) annealed materials are shown, and lines with equal power factors are plotted to give an impression of the materials' performances. The results for thin films were published by Schumacher *et al* [12].

The helium-annealed p-type materials are comparable, but the as-deposited and tellurium-annealed p-type materials show higher power factors. The power factors of as-deposited and annealed n-type nanowires are significantly higher compared to thin films, as a result of the higher electrical conductivity. As discussed above, the properties of the nanowires are measured perpendicular to the *c*-axes in the growth direction, where the electrical conductivity is higher, while the measurements of the electrical conductivity on thin films are taken in an in-plane configuration perpendicular to the growth direction. Also, the nanowires are shown to be single crystalline, while the thin films have a polycrystalline structure. This leads to higher electrical conductivities and therefore higher power factors of the nanowires, which are comparable to bulk material values. Due to its high influence on the thermoelectric properties, it can be suggested that the growth direction of electrochemically deposited thermoelectric materials has to be taken into account when constructing a device. In order to improve the performance of thermoelectric devices, the materials have to be embedded with the growth direction identical to the electrical and thermal transport direction.

4. Conclusions

We have presented the synthesis and measurements of the Seebeck coefficient as well as the electrical conductivity of individual single-crystalline $Bi_{38}Te_{55}Se_7$ and $Bi_{15}Sb_{29}Te_{56}$ nanowires as a function of temperature before and after annealing. The as-grown $Bi_{38}Te_{55}Se_7$ nanowires have a thermoelectric power factor of $S^2\sigma = 1500$ μW K^{-2} m^{-1} at room temperature; for the $Bi_{15}Sb_{29}Te_{56}$ nanowires, $S^2\sigma = 1550$ μW K^{-2} m^{-1}. In the case of $Bi_{38}Te_{55}Se_7$, annealing in a tellurium atmosphere increases the power factor by about 100%, leading to power factors comparable to nanograined bulk values. For $Bi_{15}Sb_{29}Te_{56}$, the Seebeck coefficient is increased, although the reduced electrical conductivity causes a decrease of the power factor by around 30%. The nanowires' composition and therefore their thermoelectric performance can be further improved by annealing in different atmospheres

and by the addition of other dopants. Although confinement effects if present play a negligible role, the nanowires presented here are a well-suited model system to study cross-sectional thermal transport in thermoelectric materials. For further investigations, thermal conductivity measurements by means of the 3ω method will be used for a complete ZT characterization, and this will remove the influence of geometric characterization on the thermoelectric properties.

Acknowledgments

SB and TB contributed equally to this work. The authors gratefully acknowledge the funding of the German Ministry of Education and Research (BMBF) via the project EchemTE (FKZ: 03A3542) and further financial support by the German Research Foundation (DFG) within the Priority Program SPP 1386. The authors would also like to thank Klaus-G. Reinsberg and Jose A C Broeckaert for first chemical analysis of the nanowires and for fruitful discussions.

References

[1] Nolas G S, Sharp J and Goldsmid H J 2001 *Thermoelectrics—Basic Principles and New Materials Developments vol 1* ed A Zunger, R Hull, R M Osgood and H Sakaki (Berlin: Springer) chapter 1
[2] Li D, Wu Y, Kim P, Shi L, Yang P and Majumda A 2003 *Appl. Phys. Lett.* **14** 2934
[3] Lee K-M, Lee S-K and Choi T Y 2012 *Appl. Phys.* A **106** 955–60
[4] Lee S H, Shim W, Jang S Y, Roh J W, Kim P, Park J and Lee W 2011 *Nanotechnology* **22** 295707
[5] Roh J W, Jang S Y, Kang J, Lee S and Noh J-S 2010 *Appl. Phys. Lett.* **96** 103101
[6] Dresselhaus M S and Hicks L D 1993 *Phys. Rev.* B **19** 12727–31
[7] Mavrokefalos A, Moore A L, Pettes M T, Shi L and Wang W 2009 *J. Appl. Phys.* **105** 104318
[8] Li S, Soliman H M A, Zhou J, Toprak M S, Muhammed M, Platzek D, Ziolkowski P and Müller E 2008 *Chem. Mater.* **12** 4403–10
[9] Martin-Gonzalez M S, Snyder G J, Prieto A L, Gronsky R, Sands T and Stacy A M 2003 *Nano Lett.* **3** 973–7
[10] Zimmer A, Stein N, Terryn H and Boulanger C 2007 *J. Phys. Chem. Solids* **10** 1902–7
[11] Harris C T, Martinez J A, Shaner E A, Huang J Y, Swartzentruber B S, Sullivan J P and Chen G 2011 *Nanotechnology* **22** 275308
[12] Schumacher C *et al* 2013 *Adv. Energy Mater.* **3** 95–104
[13] Yuan J H, He F Y, Sun D C and Xia X H 2004 *Chem. Mater.* **10** 1841–4
[14] Nielsch K, Choi J, Schwirn K, Wehrspohn R B and Goesele U 2002 *Nano Lett.* **2** 677–80
[15] Reinsberg K G, Schumacher C, Nielsch K and Broekaert J A C 2011 *J. Anal. Atom. Spectrom.* **26** 2477–82
[16] Fan Z, Wang D, Chang P C, Tseng W Y and Lu J G 2004 *Appl. Phys. Lett.* **24** 5923–5
[17] Rostek R, Sklyarenko V and Woias P 2011 *J. Mater. Res.* **26** 1785–90
[18] Goldsmid H J 1958 *Proc. Phys. Soc.* **7** 633–46
[19] Poudel P *et al* 2008 *Science* **320** 634–8
[20] Ma Y, Hao Q, Poudel B, Lan Y, Yu B, Wang D, Chen G and Ren Z 2008 *Nano Lett.* **8** 2580–4
[21] Kim M Y, Oh T S and Kim J S 2007 *J. Korean Phys. Soc.* **50** 760–6
[22] Yan X, Poudel B, Ma Y, Liu W S, Josh G, Wang H, Lan Y, Wang D, Chen G and Ren Z F 2010 *Nano Lett.* **10** 3373–8
[23] Delves R T, Bowley A E, Hazelden D W and Goldsmid H J 1961 *Proc. Phys. Soc.* **7** 838–44
[24] Scherrer H and Scherrer S 2006 *Thermoelectrics Handbook—Macro To Nano vol 1* ed D M Rowe (Boca Raton, FL: CRC Press) chapter 27
[25] Peranio N, Leister E, Töllner W, Eibl O and Nielsch K 2012 *Adv. Funct. Mater.* **22** 151–6
[26] Peranio N, Leister E, Töllner W, Eibl O and Nielsch K 2012 *J. Electron. Mater.* **41** 1509–12
[27] Martin-Gonzalez M S, Prieto A L, Gronsky R, Sands T and Stacy A M 2003 *Adv. Mater.* **15** 1003–6
[28] Chen Y Y, Chen C L, Lee P C and Ou M N 2011 *Nanowires—Fundamental Research* ed A Hashim (Rijeka: InTech) chapter 12